Microfluid Nanofluid (2015) 18:1095–1105
DOI 10.1007/s10404-014-1502-z

RESEARCH PAPER

Toward microfluidic design automation: a new system simulation toolkit for the in silico evaluation of droplet-based lab-on-a-chip systems

Nils Gleichmann · Daniéll Malsch · Peter Horbert · Thomas Henkel

Received: 28 April 2014 / Accepted: 7 October 2014 / Published online: 19 October 2014

Abstract Miniaturization of biological and chemical assays in lab-on-a-chip systems is a highly topical field of research. The pressure-driven droplet-based microfluidic platform is a promising way to realize these miniaturized systems by expanding the capability of assays with special features that are unreached by traditional workflows. Full custom centric design of droplet-based microfluidic lab-on-a-chip systems leads to a high system integration level and design complexity. In our work, we report on a software toolkit based on the Kirchhoff laws for modeling droplet traffic and processing for even complex microfluidic networks. Experimental validation of the simulation results was performed utilizing directional droplet transport switching in a circular channel element. This structure can be employed as a benchmark system for the experimental validation of the obtained simulation results. As a result of these experiments, our design and simulation toolkit meet the requirements for a versatile and low-risk development of custom lab-on-a-chip devices. Together with our conceptual model of microfluidic networks, most of the development problems arising with complex lab-on-a-chip applications can be solved. Due to the high computational speed, the algorithm allows an interactive in silico evaluation of even complex sample-processing workflows in droplet-based microfluidic devices prior any preparation of prototypes. Summarizing the developed toolkit may become the foundation for the future development of software tools for a microfluidic design automation. As a result of this new way of simulation-based application-driven development, the advantages of lab-on-a-chip will be accessible for more people through the easy, versatile and efficient transformation from complex laboratory workflows to compact and easy to use lab-on-a-chip applications.

Keywords Microfluidic design automation · Lab on a chip · Droplet-based microfluidics · System simulation

1 Introduction

The lab-on-a-chip concept promises to expand the capability of assays that are unreached by traditional workflows (Xize and DeMello 2012; Manz et al. 1990; Reyes et al. 2002; Figeys and Pinto 2000). A substantial aim of this technology is to bring complex laboratory workflows into small and portable devices that can be used independently from the laboratory infrastructure. This demands a genuinely problem-specific solution and accordingly application-driven development.

Besides the unique technology advantages, short development times and low costs are the users most requested features. At present, the slow and expensive development of these devices is the underlying drivers of the low uptake of this technology (Panikowska et al. 2011). Therefore, an efficient and accurate development process is the key for the common use of lab-on-a-chip technology (Oh and Furlani 2012; Boy et al. 2008; Albers and Oerding 2006). We present in this work a new way for fast and efficient application-driven development of lab-on-a-chip applications based on modeling and simulation of microfluidic networks.

Electronic supplementary material The online version of this article (doi:10.1007/s10404-014-1502-z) contains supplementary material, which is available to authorized users.

N. Gleichmann (✉) · D. Malsch · P. Horbert · T. Henkel
IPHT Jena, Albert-Einstein Straße 9, 07745 Jena, Germany
e-mail: nils.gleichmann@ipht-jena.de

The complexity of the sample-processing workflow to be implemented in lab-on-a-chip devices is constantly increasing. As a consequence, one has to deal with an increasing level of integration. Even if the channel network is built from a set of available and scalable standardized microfluidic operation units as shown in Fig. 1, its prediction and tuning becomes more and more complicated. The output of each operation unit must be compatible with the processing capabilities of the next one downstream. Because of the complex interactions between fluid–fluid interfaces and apertures, the behavior of even simple systems may be hard to predict and complex, as is widely discussed in the literature (Seemann and Herminghaus 2012; Garstecki et al. 2006).

A common development approach is the iterative optimization of the design through fabrication and testing of a prototype at each optimization step. Fabrication of prototypes costs much time and resources.

Automation techniques and new development approaches of electronic design automation (EDA) solved similar development problems for the electronic domain (Newton 1988). These automation techniques revolutionized the way of development and allowed the outstanding emergence of this technology. For a similar progress of lab-on-a-chip technology, we applied the methods of EDA to the field of microfluidic devices. The new methods and workflows are summarized in the concepts of a microfluidic design automation (MDA).

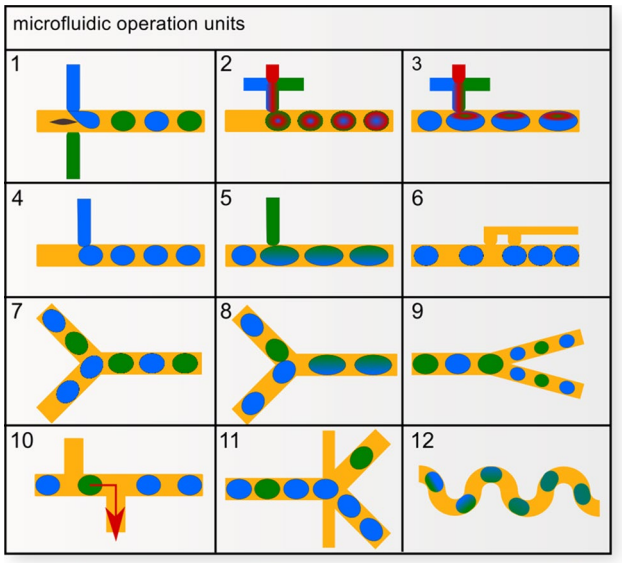

Fig. 1 Available and standardized microfluidic operation units for pressure-driven droplet-based microfluidics with models supported by the toolkit. *1*—alternating droplet generator; *2*—mixed droplet generation; *3*—mixed dosing; *4*—simple droplet generation; *5*—dosing; *6*—droplet distance control; *7*—droplet stacker; *8*—droplet merger; *9*—aliquoting; *10*—droplet retriever; *11*—sorter; *12*—mixing unit

The essential part of MDA is to enable a model-based design of complete lab-on-a-chip systems and to provide the tools for the in silico evaluation, validation and optimization of the drafted systems in a close collaboration with the customer. Our model and simulation-based development strategy makes these tools available and aims to speed up and cheapen the development process with an interactive in silico evaluation even of complex droplet-based microfluidic devices prior any preparation of prototypes. This leads to fast design optimization and thus to a faster and less expensive lab-on-a-chip development process.

As such the key for a bright future of lab-on-a-chip technologies is a fast and reliable system simulation approach. Our approach is generically usable for any thinkable custom centric microfluidic application made up of predefined, standardized, scalable functional elements (microfluidic operation units) as seen in Fig. 1. As is common in tools for EDA, the engineer creates a microfluidic network arranging the microfluidic operation units following the user-defined sample-processing workflow and simulates them by using our tools.

In our work, we present and discuss an all-in-one solution for simulation of highly integrated droplet-based microfluidic networks and the experimental validation of the correctness, exactness and computational efficiency of the obtained data utilizing directional droplet switching in a circular channel structure. This structure has been previously introduced and discussed by Fuerstman et al. (2007) as a droplet-based logic element for encoding and decoding of information by digital microfluidics.

All characteristics are implemented by mathematical expressions, which can be overridden by user-defined functions without loosing any computational efficiency.

The purpose of the toolkit is to give the microfluidic engineer a hand by simulating the complex droplet behavior in the system. The recent work is focused on modeling of droplet traffic and processing as a prerequisite for the future implementation of the chemical reaction modeling in droplets. Software interfaces for this feature are implemented as void methods. In the following part, we describe an abstract model of microfluidic networks that serves as base for our newly developed system simulation algorithm.

2 Microfluidic networks: model of lab-on-a-chip applications

The use of design automatization tools requires a formal description of the microfluidic system in a machine readable representation. An appropriate model is our newly designed microfluidic network. As example, the model of the validation system is shown in Fig. 2b. The graph

includes the microfluidic operation units and the interconnection channel network.

The microfluidic network combines information about the functional details of operation units and geometrical details of the channels. Parameters customize the function of operation units and the fluid transport in the channels. Even properties of fluids like surface tension and density are included in the model to be utilized in the simulation. In addition to this static information, dynamic aspects of the microfluidic network including hydrodynamic parameters (e.g., pressure drop and volume flow at the nodes) and the positional changes and parameters of droplets in the channels, are part of the microfluidic network. The dynamic information describes the state of the microfluidic network, and finally, a sequence of these states expresses the temporal behavior of the modeled application.

The implemented model of microfluidic networks abstracts the junction of two or three channels as a microfluidic operation unit. Their flow manipulating function is defined as a set of rules (Gleichmann et al. 2008). Because all information about the volume fractions located in the channel sections are maintained by the model of the channels, the operation units can be considered as a singular point where the channels meet. The models of the operation units are reduced to the droplet manipulation function.

The characteristics of operation units can be altered by parameters to allow them to adapt their basic functionality to the actual problem.

Similar to the EDA domain, our model provides a basic operation unit for each of the required standard operations like droplet creation, merging, splitting, separation and more (Henkel et al. 2004). Figure 1 shows operation units supported by the droplet-based microfluidics and also by our simulation toolkit. The function of the microfluidic chip device results from the combination of the function of operation units and channel functionality. Nearly, every lab-on-a-chip application can be build as a combination of these basic operation units or, respectively, represented as microfluidic network. In Fig. 2b, the illustration shows the mapping of the operation units to actual chip structures.

For each operation unit, a set of parameterizable rules is utilized to model its behavior. These rules describe both the changes of the hydrodynamic parameters and the manipulation of droplets. Besides the standard behavior given by the general rules of volume conservation, the operation unit specific rule set describes its functionality. Figure 3 shows a cutout of the rule set of the dosing operation unit. The active rule is chosen by the flow direction (A_f,B_f,C_f) and the existence of fluid–fluid interfaces (A_i,B_i,C_i). The resulting behavior is coded by the values in the columns

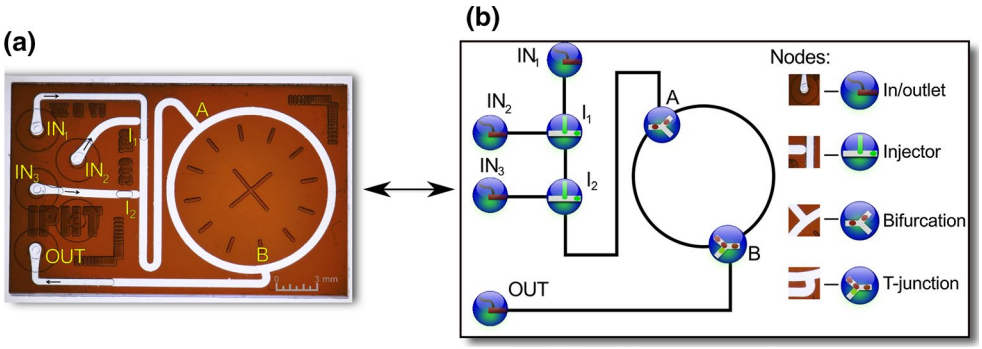

Fig. 2 A microfluidic chip device utilized as benchmark system (**a**) and the corresponding microfluidic network graph (**b**). It implements a droplet generator followed by a distance control for adjusting the droplet distance and the circular test structure for investigation of directional droplet switching

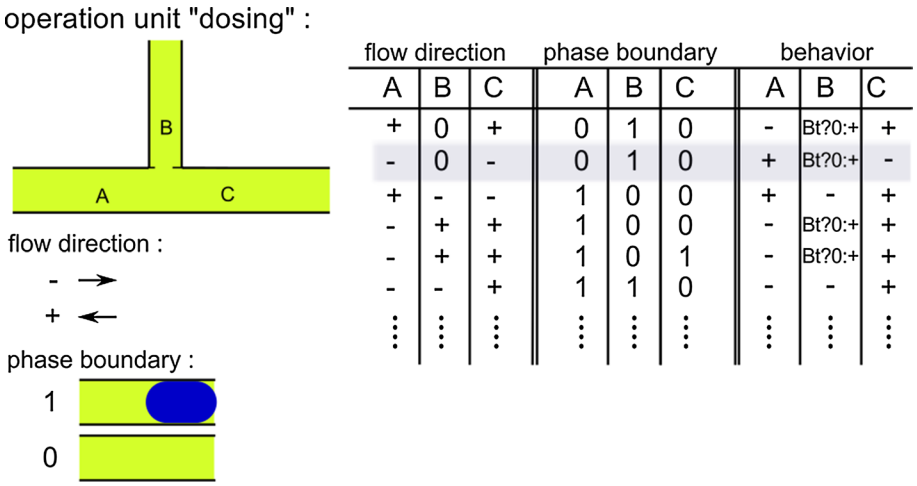

Fig. 3 Excerpt of the rules of the dosing operation unit represented as a code table. Flow direction from one of the interfaces to a channel (+ = inflow, − = outflow, 0 = no flow) and the existence of fluid–fluid interfaces (0 = none present, 1 = fluid–fluid interface) selects the appropriate behavior (− = remove volume, + = add volume—according to the volume flows, 0 = no volume flow, Bt?X:Y—if pressure hight than Laplace pressure then do X else do Y

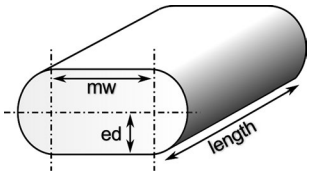

Fig. 4 Geometry parameters of a micro channel used at IPHT microfluidic devices. *mw* is the mask width, and *ed* is the etch depth. With the third parameter *length*, the channel geometry is completely parameterized

A_b,B_b,C_b. This code determines the quantity and quality of volume distribution.

As example if channel B is blocked by a droplet ($B_i = 1$), the volume streams from channel A to C ($A_f =$ "−", $B_f =$ "0", $C_f =$ "+"). This situation is highlighted in Fig. 3. This leads to a volume transport from channel A to channel C coded as $A_b =$ "−", $B_b =$ "0" and $C_b =$ "+". But the pressure in channel B can enable the droplet to overwhelm the barrier created by the channel B's aperture. In this case, the volume flow in B is not longer zero. To consider the new fact, the system parameter has to be recalculated which results in an other active rule. This pressure depended behavior is codes by the rule "Bt?0:B" in B_b.

Physical parameters such as volume flow and pressure have to be calculated for each node in the system. These values are input parameters for the rules of the operation units and define the movement and the processing of the droplets.

The geometric parameters of the channels, surface properties and the properties of used fluids define the geometry of the droplets. Figure 4 shows a cross section of the microfluidic channel used at the IPHT. A transport model developed for this channel geometry abstracts the flow between and in the droplets (Malsch 2014). This model describes how the hydrodynamic parameters depend on each other and are influenced by the droplets. Detailed description can be found in the digital supplements.

Simplified, the fluidic resistance is the sum of the Bretherton part and the Hagen–Poiseuille part. The first is generated by the moving droplet interfaces, the second by the viscous flow. Changing the transport model for other channel geometries or other flow regimes is possible by implementing the appropriate mathematical expressions.

In summary, the microfluidic network consists of two parts: a static part, describing the operation units and the channels, and a dynamic part, describing the droplets and the physical parameters at each node. The dynamic part can be subsumed as the state of the network. The transport model is defined for a specific microfluidic platform and a specific channel shape. With the modular structure, an easy adaptation is possible.

3 The simulation algorithm

As depicted in Fig. 5, our fast and efficient simulation algorithm, based on the idea of the SPICE algorithm (Nagel and Laurence 1973) for electronic circuits, is divided in four sections.

The first part analyzes the given microfluidic network and prepares this information for the nodal analysis. This results in the transfer of the operation units, segments and channels into a system of equations. It will be further optimized and solved in the second part. The result of this iterative process is the pressure drop and volume flow at every segment and operation unit in the whole system. The third part calculates the variable duration time step in which the former calculated parameters will be constant. This can be considered as the time until the next change of the system state due to influence merging or arrival of an interface at an operation unit. At this point, all parameters for the droplet manipulation are available. The fourth part updates the droplet position and processes the information about droplets according to the rules of the operation units. This new network state is the start information for the next time step until the predefined simulation time span is reached.

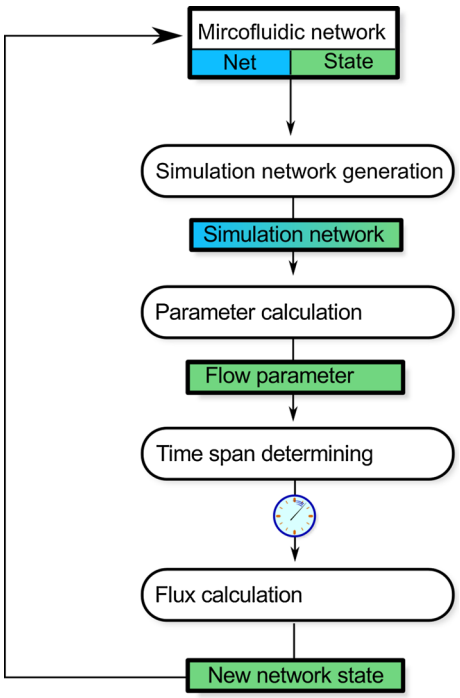

Fig. 5 A flow chart of the simulation algorithm. The user-defined microfluidic network is the starting point. It is step by step processed by the algorithm which results in a new network state, with new physical parameters and new droplet positions. The first step converts the microfluidic network in a mathematical model, describing network and state as union. It is solved in the second step. The time step length depends upon these results. The last step calculates the movement of droplets

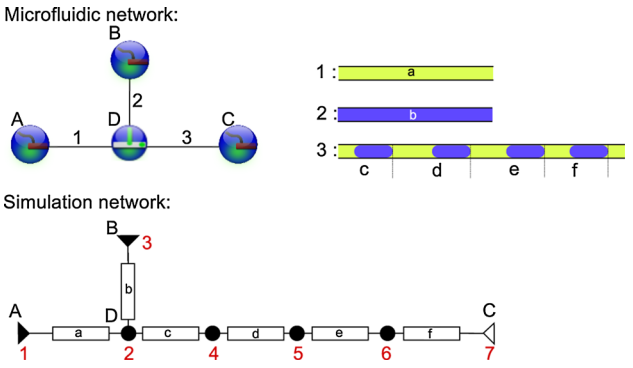

Fig. 6 Microfluidic network and its state translated into a simulation network. The simulation network unifies the static information about the network and the dynamic information about the state in one mathematical model. Each network node represents an entity influencing the hydrodynamic resistance

The simulation network generation converts the microfluidic network structure and its state from a human readable microfluidic network to the abstract computational simulation network model. This allows our new simulation algorithm to take advantage of the nodal analysis. Figure 6 shows the transformation of the static information about objects such as operation units, channels and dynamic objects such as segments to a simulation network graph. It unifies the structure and the actual state of the microfluidic network to one model.

This first step considers the various influences to the hydrodynamic resistance of a channel by the rules of the connected operation units, the fluid parameters of the contained fluid or the droplets and their parameters and the geometrical parameters of the channel.

In detail, Fig. 6 shows the creation of segment complexes (c,d,e and f) as composition of a droplet and the continuous phase between the droplets. These complexes reflect the parameters influencing the hydrodynamic resistance generated due to the flow in and between the droplets. Each segment complex has its own nonlinear hydrodynamic resistance based on the length of segments and the fluids inside the droplet and between them. Because of their nonlinear nature, they can not be easily summarized. Therefore, each segment complex gets its own node. The algorithm associates each segment complex with a hydrodynamic resistance variable in the equation system as Fig. 7 shows.

In summary, the algorithm translates the microfluidic network by inspection into a matrix and a vector by using templates without explicitly constructing the simulation network.

The second part is the solution of the systems of equations. The result contains the physical parameter space spanned by the microfluidic network. The problem, which we are dealing with, is the nonlinear hydrodynamic resistance of segmented flow. As such, the hydrodynamic resistances (R_x) are also unknown variables in the matrix.

We use a numerical linearization process to retrieve the resistance values which are valid for this network state. From an initial guess, the resistance values will be stepwise refined which includes the application of the transport model to obtain more suitable R_x values. The linearized values for R_x correspond to the real hydrodynamic resistances in the near range of the solution for P_x and $\dot{V}_x$. This process is based on the well-known Newton–Raphson algorithm, adapted to the given problem. A detailed description of our solution can be found in "Appendix 1".

The calculated stationary solution is valid for a given constant network state, or in other words, as long as no fluid–fluid interface reaches an operation unit. As a result, a rule can get activated or a new droplet configuration in the channel can be established. In these cases, the change of the physical parameters in the whole network is most likely and the network has to be recalculated. In the time span estimation section according to Fig. 5, all channels are tested for interfaces that are passing the end of that channel. Also all operation units are tested for an occurring event.

The time step duration is the shortest time which has to pass before either a droplet intersects a node or an operation unit rule demands a recalculation. During this time step, constant physical parameters are guaranteed.

The fourth part of the algorithm updates the network state by virtually moving and processing each droplet in the system according to their local velocities and the previously determined time step duration. It starts with updating the droplet position in all channels.

Figure 8 shows the segment position update process for a channel with droplets. Every segment in the channel changes its position according to the volume flow and the time step duration. This leaves a virtual "gap" at the beginning of the channel and an "overlapping" segment, like S_7 at the end. The following execution of the operation unit rules processes the overlapping segments and fills the gaps.

Every operation unit checks the condition of its rules to determine which rule is active. The rule describes the processing of the fluid volumes coming from the channels in compliance with the behavior of the underlying chip structure. The activation depends on flow direction and the presence of fluid–fluid interfaces at the entrances to the channels, as Fig. 3 shows. As example, a simple T-junction allocates the incoming fluids to the gaps on the channels according to their volume flow rates.

After the moving and processing of the droplets, a new network state is established. This new state invalidates the physical parameters calculated before. A new calculation for the next time step starts with the simulation network generation via the first part of the algorithm.

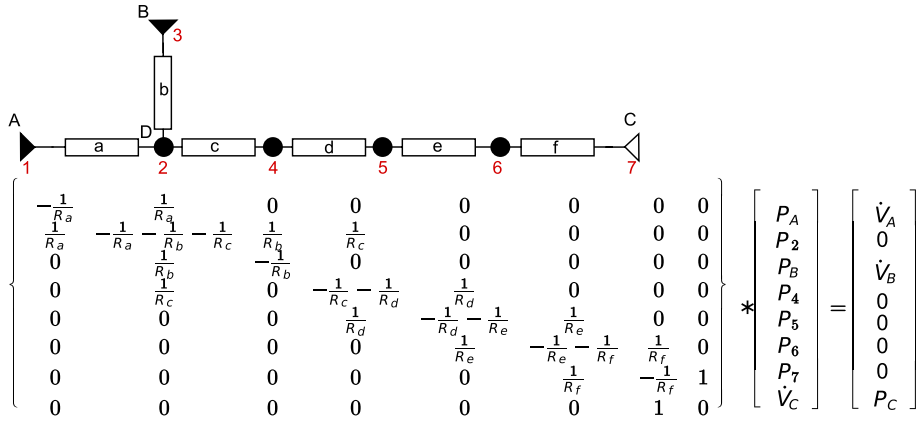

Fig. 7 Equation system for the shown simulation network. The parameter $\dot{V}_A$ is the volume flow constraint for inlet *A* as is $\dot{V}_B$ for inlet *B*. The R_x are the hydrodynamic resistances of the fluids (*a*, *b* are Hagen-Poiseuille flows) or droplets (*c*–*f*) in the channels. R_x in the result vector contains the pressure at each node, and P_C is the pressure constraint at outlet C

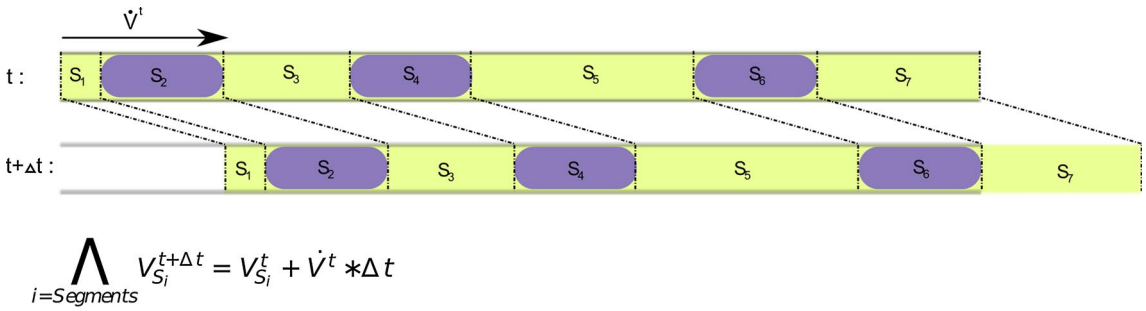

$$\bigwedge_{i=Segments} V_{S_i}^{t+\Delta t} = V_{S_i}^{t} + \dot{V}^{t} * \Delta t$$

Fig. 8 Updating the positions of segments; For every segment (S_1 … S_n) in the channel at time t, the position will be shifted by an amount depending on volume flow and time step duration

The sum of all network states over the simulation time describes the behavior of the system. Every time step contains the physical parameters and the droplet positions according to the model of microfluidic networks and the used transport equations.

4 Validation of algorithm

To determine the correctness of the algorithm for our simulation model and algorithm, we compared the simulation results with experimental measurements on a microfluidic chip device. It provides a reference system optimal for our benchmarking purpose.

This system contains a circular micro channel loop with two T-shaped junctions for inflow and outflow of droplets. Both the microfluidic network and our chip version are shown in Fig. 2. The system was previously described for investigation of droplet transport characteristics (Link et al. 2004; Fuerstman et al. 2007; Labrot et al. 2009). "Appendix 2" will give more detailed information about the setup of our experimental system.

This systems complex response behavior is the basis for its suitability as a benchmark system for our simulation tool. It is caused by the strong coupling between the flow rate in each of the branches, the number and distance of the droplets inside (Engl et al. 2005). A droplet arriving at the loop makes a binary choice to flow into the branch with lower resistance. This choice increases the resistance in the chosen branch. Each droplet continuously influences the hydrodynamic resistance by its presence in the channels. That is why each droplet changes continuously the system state. By observing the movement of droplets, these changes are indirectly measurable. The measured data can be compared to the simulated system behavior. Assumptions made about the influence of the droplet count in the branches of the loop, the droplet size, the droplet spacing, the channel geometry and the volume flow on the hydrodynamic resistance are verified by the experiments with the benchmark chip.

In detail, each droplet in a channel changes the hydrodynamic resistance by introducing liquid/liquid interfaces. (Malsch 2014). The pressure drop over both branches equals and the sum of both volume flows is constant. Hence, the change of hydrodynamic resistance results in a change of volume flow in both branches of the loop. A lower flow rate is the result of a higher hydrodynamic resistance. The observable change in droplet velocity indicates a variation of the hydrodynamic resistance. The velocity of the droplets in both branches changes with each

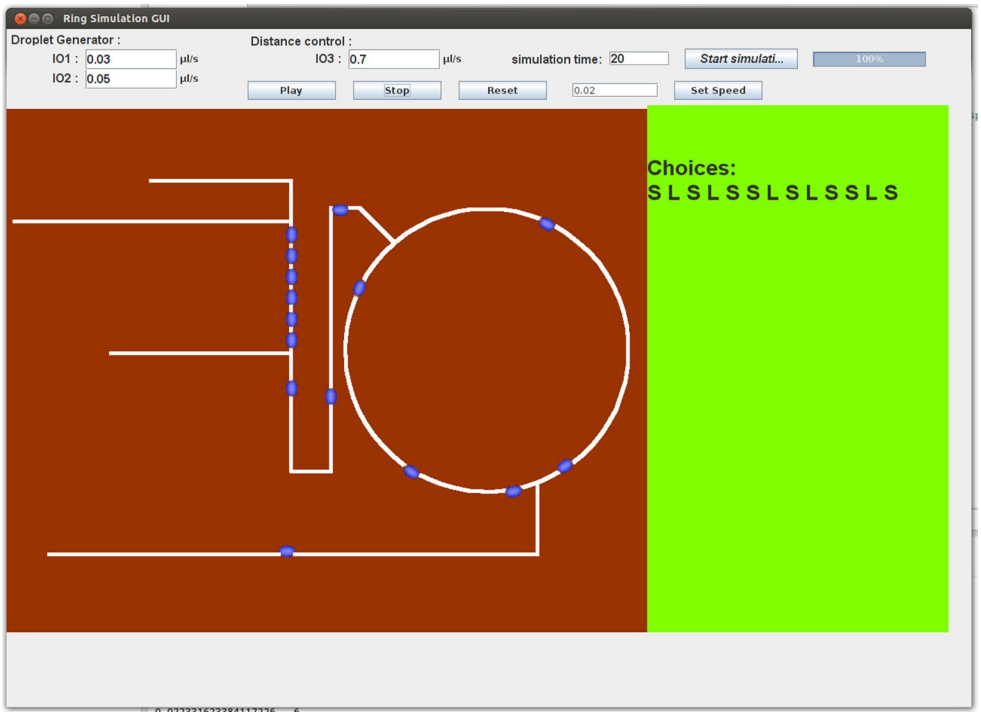

Fig. 9 The visualization tool showing the simulation of the validation system with corresponding parameters to Fig. 10. The pattern of choices is shown on the right side. *S*—short channel; *L*—long channel. The parameters IO1, IO2 and IO3 are the preset volume flow values at the interfaces of the simulated chip. Droplet sizes and spacing are simulation results

"decision" of a droplet. These back couplings induce a sensitivity to the system. Small differences in the flow conditions will lead to large changes in the sequence of droplet decisions.

For the evaluation of the validation experiments, we selected the velocity of the droplets as an indicator for the volume flow rate. This parameter allows us to measure the hydrodynamic resistance indirectly. In our experiment, a charge coupled device (CCD) camera takes pictures of the colored aqueous droplets in the channels of the chip with a frame rate of 50 fps. The resulting images are processed with a custom image processing tool based on OpenCV. We obtained the velocities of all droplets and the droplet count for each channel. In diagram 1 in Fig. 10, the experimental measured progress of the volume flow in the short and long channel between the points A and B (Fig. 2) is shown. Diagram 3 shows the numbers of droplets in each of those channels associated to diag. 1. Because the measurement approach is only applicable with droplets in the channels, the diagrams in Fig. 10 begins at the time when all considered channels include a droplet.

The simulation setup adopts all geometrical and hydrodynamic parameters according to the experimental setting. The results of the simulation are shown in Fig. 10. However, the best way for direct comparison is our visualization tool shown in Fig. 9. It visualizes the behavior of the droplets in the system. Figure 9 shows the simulation with the parameters of the experiment.

We used asymmetric loop branch lengths for our validation experiments. This predefines the path of the droplet if the count of droplets is the same in both branches. Every experiment and simulation starts with an empty loop.

With the used experimental settings, both the simulation and the experiment converge in a constant periodic sequence, as Fig. 10 shows. Other settings, which lead to more chaotic behavior, are inappropriate for validation purposes because of the instability caused by unmanageable environmental influences.

The experimental data shows the expected correlation between the droplet count and the experimental measured, respectively, simulated volume flow. Changes in the hydrodynamic resistance are reflected by changes in volume flow.

In direct comparison of experimental data in Fig. 9, the volume flow rate change happens immediately after the change in droplet count. The falling or rising edges of droplet count and volume flow rate change almost synchronously. It is a result of the negligible influence of fluid inertia.

A stable, repeatable behavior needs a constant segment length. In our validation experiments, the deviation of segment lengths after the second injector was ± 2.7 %. This resulted from the unstable volume flow rate at the three inlets of the system. As mentioned, slight variations can cause totally different system behaviors. Therefore, we chose an experimental setting with a high stability. We used an average droplet spacing of 6.69 mm because the events are not too close to each other, so unintended experimental influences do not change the results significantly.

The droplet count diagram (3 and 4 in Fig. 10) represents the droplets' decision sequence and also the behavior of the

system. So the almost equal graphs for the simulation and the experiment also indicate the conformity between them.

The comparison between the simulation and the experiment exposes the nearly identical behavior of both. The differences in droplet timing entering or leaving the loop are a result of the high sensitivity to small differences. Experimental uncertainties can lead to a minimal delay in the droplet timing for a split second which results in a different behavior of the whole system.

Despite of these effects, the results of the experiments and simulations shown in the diagrams in Fig. 10 offer equal behavior of the volume flow rate as a result of the changes in droplet count. This implicates the conformity of the simulation and the experiment. So the simulation algorithm, the underlying models and the virtual droplet processing have been validated.

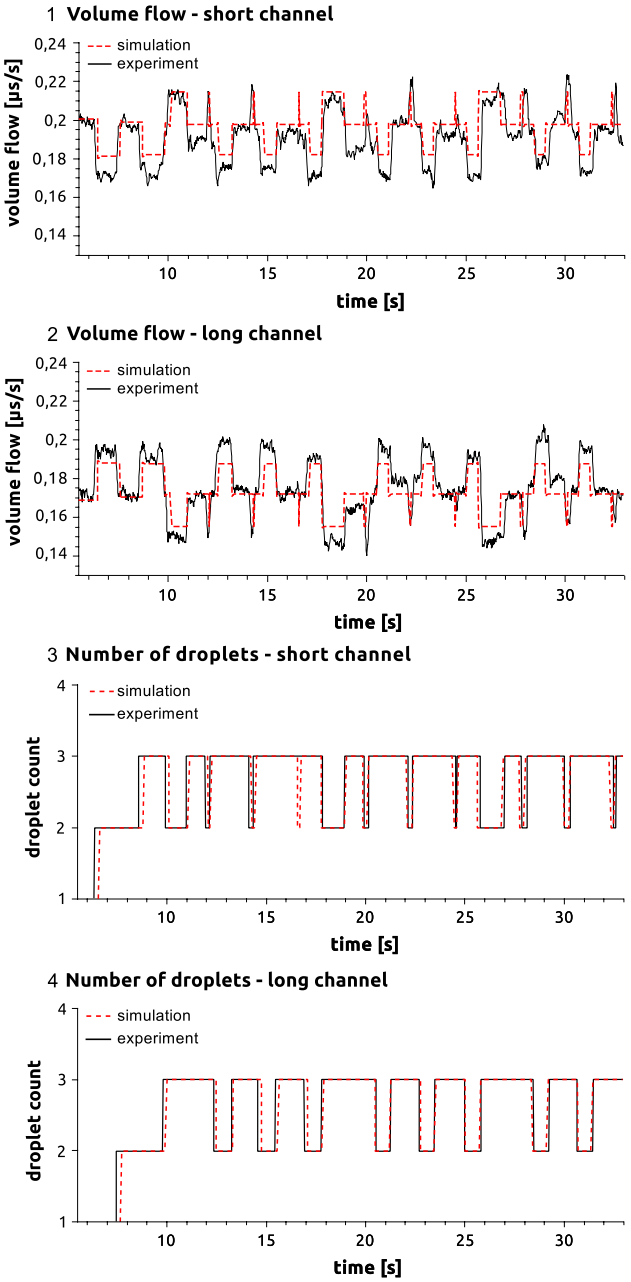

Fig. 10 Comparison between experimental results and simulation results. As seen in *3* and *4*, the numbers of droplets behave in the same way. This behavior is based on the volume flow (*1* and *2*) which is almost the same in the experiment and the simulation

5 Computational costs

For the simulated benchmark system, the calculation speed is twice as fast as the experiment. The detailed speed assessment of the algorithm is evaluated for both the simulation of an example system and the analysis of the algorithm.

For first consideration, we used a test system for the simulation which contains an injector for droplet creation and a long channel behind it. The system constantly increases the number of droplets. We measured the computational time to solve the system for every new network state for every part of the algorithm showed in Fig. 5.

The computational time depends mainly on the number of nodes in the simulation network. With each additional droplet, the network grows. The number of operation units, the second source of simulation network nodes, remains constant. Therefore, the dependency between simulation time and the number of droplets is a good indicator of the algorithm's time costs. All other influences have a negligible impact on the calculation time.

As the results of measurement in Fig. 11 reveals, the calculation of the physical parameters consumes most of the calculation time. This part of the algorithm dominates the computational time of the whole algorithm. The experimental data reflects the polynomial dependency $O(n^m)$ (with $m \in \mathbb{Z}$) between computational time and the number of segments n.

The theoretical evaluation of the algorithm reveals a computational cost in $O(n^3)$ with n as the number of segments. The part with the highest costs, the computation of the physical parameters, has an effort of $O(n^3)$. It contains the Newton–Raphson algorithm including the solution of a linear equation system with the LU-decomposition. The cost for the solution of the equation system is approximately $2/3n^3$, if the matrix has the size n. The cost of the Newton–Raphson method, which does the linearization of the hydrodynamic resistance, is in $O(\log(m) \times F(m))$ with m as the digit-precision. m is independent of the number of segments and constant. This results in a constant factor for the cost for the LR-decomposition. Therefore, the summarized time complexity for the whole step is in $O(n^3)$.

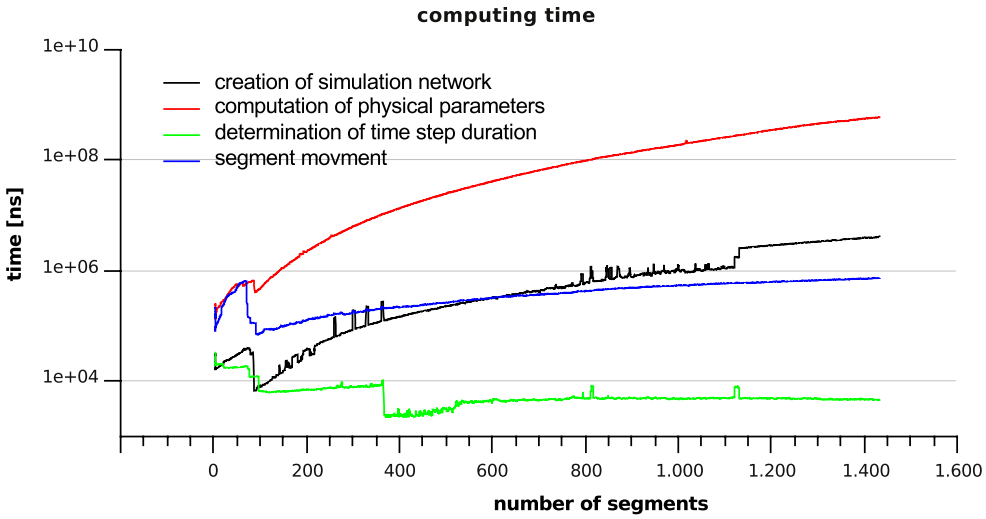

Fig. 11 Computing time for the simulation algorithm split into the four parts. This shows the polynomial dependency between number of segments and computing time

Practically, with typically up to 500 droplets in a lab-on-a-chip application, an acceptable calculation speed for development purposes is achieved. As example, it is possible to simulate a complex systems behavior for 60 s for validation in less than half a minute on a AMD Phenom(tm) 9650 2.3 Ghz. So the developer can use a design–test–redesign work flow without pauses imposed by simulation duration.

6 Conclusion

The slow and inefficient development of application-specific lab-on-a-chip devices generates the stringent necessity for a new development strategy. The key requirement for this important step beyond the frontiers of manual development is a fast and correct working simulation ability.

The new simulation algorithm described above offers all these capabilities for the microfluidic platform of pressure-driven droplet-based lab-on-a-chip technology. Its main advantage over other simulation methods is its unrivaled speed and performance, which is essential for the microfluidic design automation. The microfluidic network as underlying model and the formal description language enables a way of easy communication between the customer and the developer. Along with the simulation algorithm implemented in a tool, the formal model language paves the way for an in-time development with strong user integration.

These practical advantages woven into the tapestry of an efficient development procedure greatly reduces the development risks. Shorter and even more successful development of droplet-based lab-on-a-chip devices opens the technology for more users and their application ideas.

Our algorithm is based on a modular design. With our versatile concept of basic operation units and the transport model condensed in the model of microfluidic networks, it is easy to integrate other microfluidic technologies.

In summary, we have provided a new, efficient method for the development of lab-on-a-chip devices. The advantages of lab-on-a-chip will be accessible for more people through the easy, versatile and efficient transformation from complex laboratory workflows to compact and easy to use lab-on-a-chip applications.

Acknowledgments This work was supported by the BMBF in the projects DiNaMiD(0315591B/BMBF) and BactoCat (031A161A/BMBF).

Appendix 1: Linearization and solution of the equation system built from the microfluidic network

The equation system in matrix form contains the physical parameter space spanned by the microfluidic network. Preset by the user are the constraints $\dot{V}_A, \dot{V}_B, \dot{P}_C$. The calculation results will be held in the result vector's elements $P_A, P_2, P_B, P_4, P_5, P_6, P_7, \dot{V}_C$ for each node, which represents an operation unit or a droplet. $R_{a,b,c,d,e,f}$ represents the dynamic hydrodynamic resistance and $\dot{V}_{2,4,5,6}$ represents the calculated volume flow at each node.

The solution of the equation system in the bottom of Fig. 7 evaluates all parameters for the microfluidic network with the given hydrodynamic resistances R_x. The problem is to find the correct values for R_x. As mentioned, the hydrodynamic resistance of droplets is not linear, but the linearity of the R_x values is the basis of the nodal analysis

algorithm. Figure 12a shows the nonlinear dependency of R for a droplet. Other parameters such as channel geometry, droplet complex length and fluid properties also influence the hydrodynamic resistance, but are considered as constant in this analysis. Only the relation between $\dot{V}$ and ΔP is considered. The parameter R_{linear}, which is used to describe the network as system of equations, describes a linear dependency as seen in Fig. 12b. R_{linear} is the slope given by the first derivative of the real hydrodynamic resistance function at the given point ΔP_w. The second part of the algorithm finds a correct value for R_{lin} and so the correct $\Delta P, \dot{V}$ pair with the numerical methods.

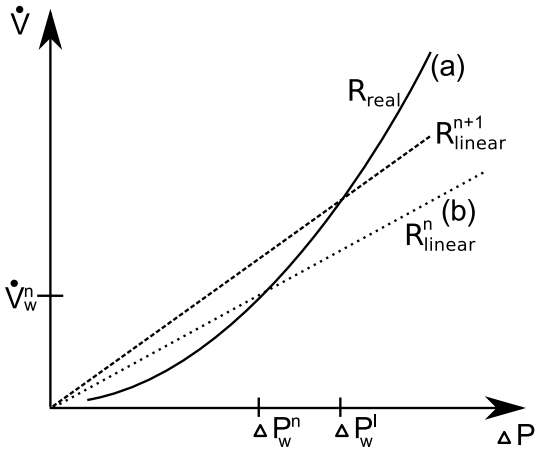

Fig. 12 (*a*) Example for the nonlinear dependency of resistance (R_{real}) for a droplet complex. (*b*) the linearized resistance for the point w in iteration n is defined by the $R^n_{\text{linear}} = \frac{d\dot{V}(\Delta P)}{\Delta P}$ at P_w $\Delta P'_w$ is the result solving the system matrix (Fig. 7). Its a new working point closer to the solution. R^{n+1}_{linear} is used as the new linearized resistance dependency in the next iteration $n+1$

The algorithm starts with an initial guess for the resistance parameter R_x. This guess will be optimized iteration by iteration with the solution of the equation system generated an iteration before.

Every iteration step calculates new values for pressure drop and volume flow of each node, based on the approximation of the node's hydrodynamic resistance. We applied the equation of the transport model, which is discussed earlier and shown in Fig. 12a, on these new values to get a new linear approximation of the hydrodynamic resistance. The error of the new approximation is smaller than before, because the new approximation point ΔP_w is closer to the final solution.

After some optimization steps, the algorithm finds an approximation for R_x that fulfills the precision requirements. The result is a $R_x = \frac{\Delta P}{\dot{V}}$ value which matches the real nonlinear hydrodynamic resistance around the values ΔP and $\dot{V}$. The use of the equation system solved as matrix equation ensures that the pressure drop including the hydrodynamic resistance and the volume flow for all channels and droplets are optimized at once. At the end, all R_x match the real hydrodynamic resistances at ΔP_x and $\dot{V}_x$.

The algorithm performs this optimization for all droplet complexes simultaneously. If the maximal error of the approximations is smaller than a predefined accuracy criterion, the calculation of the physical flow parameter $\dot{V}$ and P for each node is done.

Appendix 2: experimental validation system

All-glass technology was selected for fabrication of the optical transparent microchannel system for validation. Half channels following the design in Fig. 13 were etched

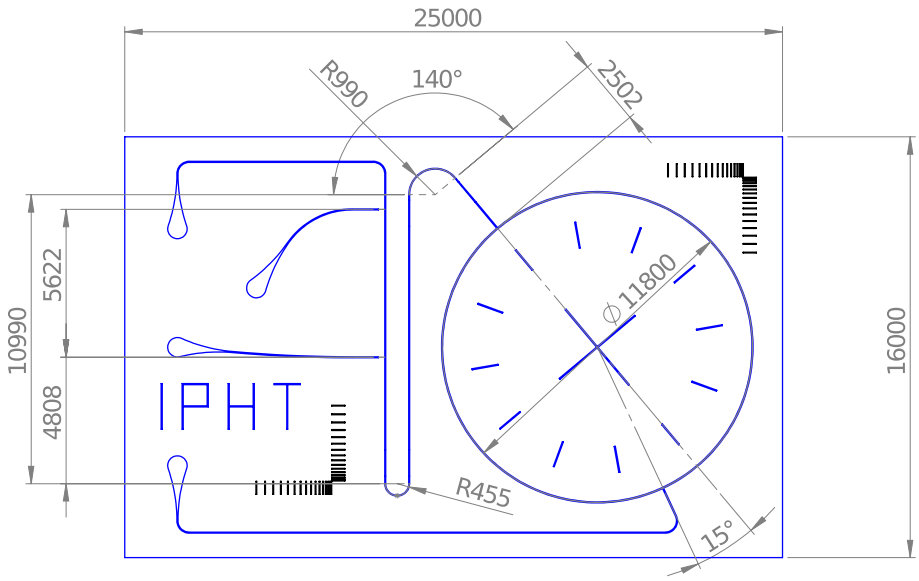

Fig. 13 Layout for the validation system. Measurements are given in µm

with hydrofluoric acid into glass substrates. A mask aligner aligned two of them. In the next step, an anodic bonding process merged two chip halves together with help of a bond support layer of 100 nm silicon. This layer was removed from the channel walls by etching, which provides the optical transparency for the micro channels.

The transport of the droplet sequences demands the cross section shown in Fig. 4 to avoid bypass flow of the separation fluid. An etch depth of 130 µm and a mask wide of 40 µm results in an almost circular channel profile. Its height is 260 µm, and its width is 300 µm.

A lubrication layer prevents direct contact between the dispersed phase and the microchannel walls. It is facilitated by hydrophobic surface functionalization using alkyl silanes.

The microfluidic chip is made for optimal optical access to the droplet content. It is 1.4 mm thick, and its planar dimensions are 25 mm × 16 mm. The length of the channels between the functional elements like injectors or bifurcation is given by the draft displayed in Fig. 13.

References

Albers A, Oerding J (2006) Product development regarding micro specific tasks. Microsyst Technol 16:1537–1545. doi:10.1007/s00542-010-1042-8

Boy DA, Gibou F, Pennathur S (2008) Simulation tools for lab on a chip research: advantages, challenges, and thoughts for the future. Lab Chip 8(9):1424–1431. doi:10.1039/16812596c

Engl W, Roche M, Colin A, Panizza P, Ajdari A (2005) Droplet traffic at a simple junction at low capillary numbers. Phys Rev Lett 95(20):208304. doi:10.1103/PhysRevLett.95.208304

Figeys D, Pinto D (2000) Lab-on-a-chip: a revolution in biological and medical sciences. Anal Chem 72(9):330A–335A. doi:10.1021/ac002800y

Fuerstman MJ, Garstecki P, Whitesides GM (2007) Coding/decoding and reversibility of droplet trains in microfluidic networks. Science 315(5813):828–832. doi:10.1126/science.1134514

Garstecki P, Fuerstman MJ, Stone HA, Whitesides GM (2006) Formation of droplets and bubbles in a microfluidic T-junction—scaling and mechanism of break-up. Lab Chip 6(3):437–446. doi:10.1039/B510841A

Gleichmann N et al (2008) Toolkit for computational fluidic simulation and interactive parametrization of segmented flow based fluidic networks. Chem Eng J 135(2008):S210–S218

Henkel T, Bermig T, Kielpinski M, Grodrian A, Metze J, Köhler JM (2004) Chip modules for generation and manipulation of fluid segments for micro serial flow processes. Chem Eng J 101(1–3):439–445. doi:10.1016/j.cej.2004.01.021

Labrot V, Schindler M, Guillot P, Colin A, Joanicot M (2009) Extracting the hydrodynamic resistance of droplets from their behavior in microchannel networks. Biomicrofluidics 3(1):012804

Link DR, Anna SL, Weitz DA, Stone HA (2004) Geometrically mediated breakup of drops in microfluidic devices rid b-6435-2008. Phys Rev Lett 92(5):054503

Malsch D (2014) Strömungsphänomene der Tropfenbasierten Mikrofluidik. Disseration, Technische Universität Ilmenau

Manz A, Graber H, Widmer HM (1990) Miniaturized Total Chemical Analysis Systems: A Novel Concept for Chemical Sensing. Sensor Actuator B-Chem 1(1–6):244–248. doi:10.1016/0925-4005(90)80209-I

Nagel LW (1973) SPICE (Simulation Program with Integrated Circuit Emphasis). Tech Rep EECS Department, University of California, Berkeley

Newton AR (1988) Twenty-five years of electronic design automation. Proc 25th ACM/IEEE Design Automation Conference, 2. DAC'88. Los Alamitos, CA, USA: IEEE Computer Society Press. http://dl.acm.org/citation.cfm?id=285730.286213

Oh KW, Furlani EP (2012) Design of pressure-driven microfluidic networks using electric circuit analogy. Lab Chip 3(12):515–545

Panikowska K, Ashutosh T, Alcock J (2011) Towards service-orientation—the state of service thoughts in the microfluidic domain. Int J Adv Manuf Technol 56(1):135–142. doi:10.1007/s00170-011-3171-3

Reyes DR, Iossifidis D, Auroux PA, Manz A (2002) Micro total analysis systems. 1. Introduction, theory, and technology. Anal Chem 74(12):2623–2636. doi:10.1021/ac0202435

Seemann R, Herminghaus S (2012) Droplet based microfluidics. Reports on Progress in Physics (1/75) http://iopscience.iop.org/0034-4885/75/1/016601

Xize N, DeMello AJ (2012) Building droplet-based microfluidic systems for biological analysis. Biochem Soc Trans 4(40):615–623. doi:10.1042/BST20120005